A Clinical Feasibility Study to Image Angiogenesis in Patients with Arteriovenous Malformations Using ^{68}Ga-RGD PET/CT

Daphne Lobeek[1], Frédérique C.M. Bouwman[1], Erik H.J.G. Aarntzen[1], Janneke D.M. Molkenboer-Kuenen[1], Uta E. Flucke[2], Ha-Long Nguyen[3], Miikka Vikkula[3,4], Laurence M. Boon[3,4], Willemijn Klein[1,5], Peter Laverman[1], Wim J.G. Oyen[1,6,7], Otto C. Boerman[1], Samantha Y.A. Terry[8], Leo J. Schultze Kool[1,5], and Mark Rijpkema[1]

[1]Department of Radiology and Nuclear Medicine, Radboud University Medical Center, Nijmegen, The Netherlands; [2]Department of Pathology, Radboud University Medical Center, Nijmegen, The Netherlands; [3]Human Molecular Genetics, de Duve Institute, University of Louvain, Brussels, Belgium; [4]Centre for Vascular Anomalies (part of VASCERN European Reference Network), Division of Plastic Surgery, Cliniques Universitaires Saint-Luc, Brussels, Belgium; [5]Centre for Vascular Anomalies (part of VASCERN European Reference Network), Department of Radiology and Nuclear Medicine, Radboud University Medical Center, Nijmegen, The Netherlands; [6]Department of Biomedical Sciences, Humanitas University, Milan, Italy; [7]Department of Radiology and Nuclear Medicine, Rijnstate Hospital, Arnhem, The Netherlands; and [8]Department of Imaging Chemistry and Biology, School of Biomedical Engineering and Imaging Sciences, King's College London, London, United Kingdom

Arteriovenous malformations (AVMs) have an inherent capacity to form new blood vessels, resulting in excessive lesion growth, and this process is further triggered by the release of angiogenic factors. ^{68}Ga-labeled arginine-glycine-aspartate tripeptide sequence (RGD) PET/CT imaging may provide insight into the angiogenic status and treatment response of AVMs. This clinical feasibility study was performed to demonstrate that ^{68}Ga-RGD PET/CT imaging can be used to quantitatively assess angiogenesis in peripheral AVMs. **Methods:** Ten patients with a peripheral AVM (mean age, 40 y; 4 men and 6 women) and scheduled for endovascular embolization treatment were prospectively included. All patients underwent ^{68}Ga-RGD PET/CT imaging 60 min after injection (mean dose, 207 ± 5 MBq). Uptake in the AVM, blood pool, and muscle was quantified as SUV_{max} and SUV_{peak}, and a descriptive analysis of the PET/CT images was performed. Furthermore, immunohistochemical analysis was performed on surgical biopsy sections of peripheral AVMs to investigate the expression pattern of integrin $\alpha_v\beta_3$. **Results:** ^{68}Ga-RGD PET/CT imaging showed enhanced uptake in all AVM lesions (mean SUV_{max}, 3.0 ± 1.1; mean SUV_{peak}, 2.2 ± 0.9). Lesion-to-blood and lesion-to-muscle ratios were 3.5 ± 2.2 and 4.6 ± 2.8, respectively. Uptake in blood and muscle was significantly higher in AVMs than in background tissue ($P = 0.0006$ and $P = 0.0014$, respectively). Initial observations included uptake in multifocal AVM lesions and enhanced uptake in intraosseous components in those AVM cases affecting bone integrity. Immunohistochemical analysis revealed cytoplasmatic and membranous integrin $\alpha_v\beta_3$ expression in the endothelial cells of AVMs. **Conclusion:** This feasibility study showed increased uptake in AVMs with angiogenic activity, compared with surrounding tissue without angiogenic activity, suggesting that ^{68}Ga-RGD PET/CT imaging can be used as a tool to quantitatively determine angiogenesis in AVMs. Further studies will be conducted to explore the potential of ^{68}Ga-RGD PET/CT imaging for guiding current treatment decisions and for assessing response to antiangiogenic treatment.

Key Words: arteriovenous malformation; PET/CT; RGD; integrin $\alpha_v\beta_3$; angiogenesis

J Nucl Med 2020; 61:270–275
DOI: 10.2967/jnumed.119.231167

Arteriovenous malformations (AVMs) are tangles of shunting blood vessels (nidus) in which the arteries are directly connected to a venous drainage network (*1*). AVMs are highly complex structures in which angiogenic stimuli act in dynamic interplay with local hemodynamic conditions (*2,3*). Patients commonly present with deformations, abnormal pulsating masses, pain, hemorrhage, or ulcers at ages ranging from youth to middle age (*4*). When AVMs are left untreated, loss of organ function, cardiac overload, skin necrosis, or bleeding are serious complications. AVMs can manifest throughout the body, but their effect on quality of life can be devastating when they are on the face (resulting in a severe cosmetic defect) or on the extremities (impairing mobility).

Current treatment options for these congenital anomalies are still limited to either surgical removal of the nidus or occlusion of the nidus through endovascular embolization. Unfortunately, both treatments have drawbacks and may show only a partial response or severe damage to the surrounding tissues (*5,6*). Furthermore, these interventions may cause hemodynamic changes to the AVM, initiating progression of disease at adjacent sites, increasing the risk of complications, destabilizing the AVM, and creating a subsequent need for repeated interventions (*6*).

Recent advances in the understanding of AVM-related angiogenesis have stimulated discussion on the use of systemic drugs targeting angiogenesis (*7,8*). However, effective application of antiangiogenic drugs to patients is hampered by a lack of tools to assess the presence and dynamics of angiogenesis within the AVM during the course of the disease. Therefore, molecular imaging techniques enabling visualization of angiogenesis are warranted to provide clinicians with quantitative outcome measures to monitor follow-up of treatment efficacy or to predict response to (antiangiogenic) treatment.

Received May 15, 2019; revision accepted Jul. 8, 2019.
For correspondence or reprints contact: Daphne Lobeek, Department of Radiology and Nuclear Medicine, Radboud University Medical Center, P.O. Box 9101, 6500HB, Nijmegen, The Netherlands.
E-mail: daphne.lobeek@radboudumc.nl
Published online Sep. 13, 2019.

Integrin $\alpha_v\beta_3$, expressed on the activated endothelial cells of newly formed blood vessels, is an attractive target for radiopharmaceuticals, allowing quantitative molecular imaging of angiogenesis using radiolabeled arginine-glycine-aspartate tripeptide sequence (RGD) derivatives and PET/CT (*9,10*). ^{68}Ga-labeled dimeric RGD (^{68}Ga-RGD) is a radiopharmaceutical that binds integrin $\alpha_v\beta_3$ with high affinity and has shown potential for tumor imaging (*11–14*). Because the development of AVMs is closely related to angiogenesis, ^{68}Ga-RGD PET/CT imaging may enable quantitative assessment of angiogenesis in peripheral AVMs. The aim of this study was to assess integrin $\alpha_v\beta_3$ expression levels in peripheral AVMs and determine the feasibility of using ^{68}Ga-RGD PET/CT imaging to visualize angiogenesis in peripheral AVMs.

MATERIALS AND METHODS

Study Population

This prospective proof-of-concept study was approved by the regional Ethics Review Board. The study (EudraCT 2015-005809-36) is registered in the Dutch trial register as number NL56104.091.16. Written informed consent was obtained from all participants. All procedures were in accord with the ethical standards of the institutional and national research committee and with the 1964 Helsinki declaration.

Patients diagnosed with at least 1 peripheral AVM confined to the subcutaneous or muscle tissue, with or without an intraosseous component, were included. AVMs were classified by their flow dynamics, clinical behavior, and angioarchitecture according to the Yakes classification (*15*). Patients were eligible if preoperative imaging of the lesion (4-dimensional CT angiography [4D-CTA] and angiographic imaging) was available, and patients were scheduled for percutaneous or transarterial embolization treatments with ethanol. Patients with contraindications to ^{68}Ga-RGD PET/CT imaging (pregnancy, breastfeeding, or severe claustrophobia) or with impaired renal or liver function (creatinine clearance $\leq$ 60 mL/min, aspartate aminotransferase and alanine aminotransferase levels $\geq$ 3 times the upper limit of normal, and total bilirubin $\geq$ 2 times the upper limit of normal) were ineligible. When ^{68}Ga-RGD PET/CT imaging was performed between 2 treatments, imaging was scheduled at least 6 wk after the last treatment to minimize potential uptake related to treatment-associated inflammation.

^{68}Ga-RGD PET/CT Acquisition

Patients were intravenously administered 207 ± 7 MBq (42 ± 8 μg) of ^{68}Ga-RGD (range, 197–215 MBq [34–58 μg]) using a slow bolus injection of 8 mL over 1 min. Preparation of the radiotracer is described in the supplemental material (available at http://jnm.snmjournals.org). Patients had no restrictions on food or medicine intake and were asked to void before undergoing scanning. At 61 ± 6 min after injection, ^{68}Ga-RGD PET/CT images were acquired using a Biograph 40 mCT scanner (Siemens Healthcare). A low-dose CT scan (512 × 512 voxels; voxel size, 0.98 × 0.98 × 5 mm; pitch, 1; 16 × 1.2 mm) was acquired for attenuation correction and as an anatomic reference, with an automatically modulated x-ray tube voltage and current (120 kV, 50 mA) using Care kV and Care Dose4D (Siemens Healthcare). The PET images were acquired in list mode at 10 min per bed position, with the field of view covering the entire AVM (200 × 200 matrix; voxel size, 4.07 × 4.07 × 5 mm; 2–3 bed positions covering a 225- to 725-mm field of view). The CT images were reconstructed with a B31f convolution kernel. The PET images were reconstructed using a 3-dimensional ordered-subset expectation maximization algorithm with a spatially varying point-spread function incorporating time-of-flight information (3 iterations and 21 subsets, a 200 × 200 matrix, and a 2.04-mm pixel size). A 3-dimensional gaussian filter kernel of 3.0 mm in full width at half maximum and a transaxial matrix of 200 × 200 mm were used as a postreconstruction filter.

Safety analysis included recording adverse events according to the Common Terminology Criteria for Adverse Events, version 4.03; recording changes in vital signs (blood pressure, temperature, and heart rate) before and up to 2 h after radiotracer injection; and obtaining laboratory measurements (hemocytology, kidney function [creatinine clearance and urea], and liver function [aspartate aminotransferase level, alanine aminotransferase level, and total bilirubin]) at baseline and 1 wk after radiotracer injection. A study flowchart is provided in Supplemental Figure 1.

^{68}Ga-RGD PET/CT Image Analysis

Visual image analysis and AVM detection were performed using Oasis software (version 1.9; Segami Corp.). PET quantification was performed with Inveon Research Workspace software (version 2.04; Siemens). When patients showed multiple AVMs, only the AVM that was or would be embolized was delineated. For uptake in muscle and arterial tissue, a spheric volume of interest with a 3-cm diameter was defined manually in CT images and subsequently transferred to the registered PET images. The segmentation of this volume of interest depended on the location of the AVM and its surrounding tissue within the PET field of view. To determine the relationship of pathologic uptake to physiologic uptake in the liver, spleen, mediastinum, and kidney, spheric volumes of interest were drawn in these areas. The information within all volumes of interest was subsequently exported to MATLAB, version R2014b (The MathWorks) to calculate SUV_{max} and SUV_{peak}. SUV_{peak} was determined using in-house–developed software by generating an SUV_{mean} for the voxel with the highest uptake (SUV_{max}) and its surrounding voxels within a 1 cm^3 sphere. Lesion-to-blood and lesion-to-muscle ratios were calculated, respectively, as follows:

$$\frac{SUV_{peak,lesion}}{SUV_{peak,blood}} \text{ and } \frac{SUV_{peak,lesion}}{SUV_{peak,muscle}}.$$

Immunohistochemical Analysis

Five-micrometer sections of frozen (n = 3) and paraffin-embedded (n = 7) surgical biopsy material from the lip, orbita, cheek, finger, foot, lower leg, and back of peripheral AVMs was used for immunohistochemical analysis. Tissue samples were stained for integrin $\alpha_v\beta_3$ expression (anti-$\alpha_v\beta_3$ integrin monoclonal antibody, MAB1976B, clone LM609, 10 μg/mL [Merck Millipore] [frozen sections], and AB7166, clone BV3, 1:100, [Abcam] [paraffin sections]), microvascular density (anti-CD31 monoclonal antibody, 1:50, ab28364 [Abcam]), and hematoxylin and eosin. Evaluation by light microscopy was performed, in which staining patterns, including patterns in the endothelium of vessels or normal tissues, were assessed.

Statistical Analysis

Values are represented as mean ± SD. Graphs were made and statistical analyses of SUV_{peak} were performed using Prism, version 5.03 (Graph Pad Software, Inc). Differences in background tissue uptake were tested for significance using a 1-way ANOVA with post hoc Bonferroni adjustments. Statistically significant differences between pathologic uptake and physiologic background uptake were tested using a paired-sample t test. An α-value of 0.05 was used in all analyses. Patterns of staining were scored semiquantitatively according to intensity and extent in the whole slide (0, no staining; 1, weak staining; 2, moderate staining; and 3, strong staining).

RESULTS

Patient Population

Six women and 4 men (mean age, 43 y ± 17 and 34 y ± 8, respectively) participated in this pilot study. The patient characteristics are given in Table 1. One patient (patient 7) underwent ^{68}Ga-RGD PET/CT imaging before a first endovascular embolization

TABLE 1
Patient Characteristics

Patient no.	Age (y)	Sex	Yakes classification (*15*)	Location AVM
1	28	Male	IIIb	Chin
2	27	Male	II	Nose
3	44	Male	II	Right foot
4	51	Female	II	Finger, digit I, right
5	64	Female	II	Finger, digit II, right
6	57	Female	II	Finger, digit V, left
7	38	Male	IIIa	Right lower leg
8	26	Female	II	Left upper leg
9	38	Female	II	Right hand
10	23	Female	II	Right elbow

therapy, 4 patients (patients 1, 2, 5, and 10) underwent imaging on average 2.5 mo (range, 2–3 mo) after the last treatment, and 3 patients (patients 3, 8, and 9) were scheduled for a new treatment after 9 mo because of underlying complications. One patient (patient 4) underwent imaging 6 mo after the last intervention, but during the next intervention no nidus was found and therefore embolization could not be performed. One patient (patient 6) showed slowly progressive disease (increased pain) and underwent imaging before the first embolization therapy after 8 y.

^{68}Ga-RGD PET/CT Imaging of AVM

There were no clinically detectable adverse events, or injected-related (serious) adverse events, or any changes in vital signs in any of the subjects. Blood analysis before and 1 wk after ^{68}Ga-RGD tracer injection showed laboratory values within reference ranges; no clinically relevant changes were observed.

All lesions, as defined on conventional angiographic images, could readily be identified on ^{68}Ga-RGD PET/CT scans independently of the location or size of the AVM, with lesion-to-blood and lesion-to-muscle ratios of 3.5 ± 2.2 and 4.6 ± 2.8, respectively. In all patients, radiotracer accumulation corresponded to the location of the nidus as defined by plain angiographic and 4D-CTA images (Fig. 1). The mean SUV_{max} and SUV_{peak} were 3.0 (range, 1.0–4.6) and 2.2 (range, 0.7–3.6), respectively. Uptake within the lesion was significantly higher than radioactivity levels in the blood ($P = 0.0014$) and the muscle ($P = 0.0006$). The SUV_{peak} for ^{68}Ga-RGD uptake in all AVMs and normal tissues is shown in Figure 2. Uptake in the blood pool and muscle was comparable in all patients, even with variances in blood-pool and muscle selection. Mean uptake did not significantly differ between the blood pool and muscle ($P = 0.11$). An example of the range of physiologic uptake in different organs is provided in Supplemental Figure 2.

In 9 of 10 patients, the hot spots in the ^{68}Ga-RGD PET/CT images colocalized with the center of the AVM as revealed on 4D-CTA and angiographic images. Interestingly, ^{68}Ga-RGD PET/CT images revealed a PET-positive lesion within the palmar side of the right hand of patient 9, whereas angiographic imaging did show a diffuse and complex AVM with multiple enlarged feeding arteries and a pattern of increased venous drainage without a clear nidus.

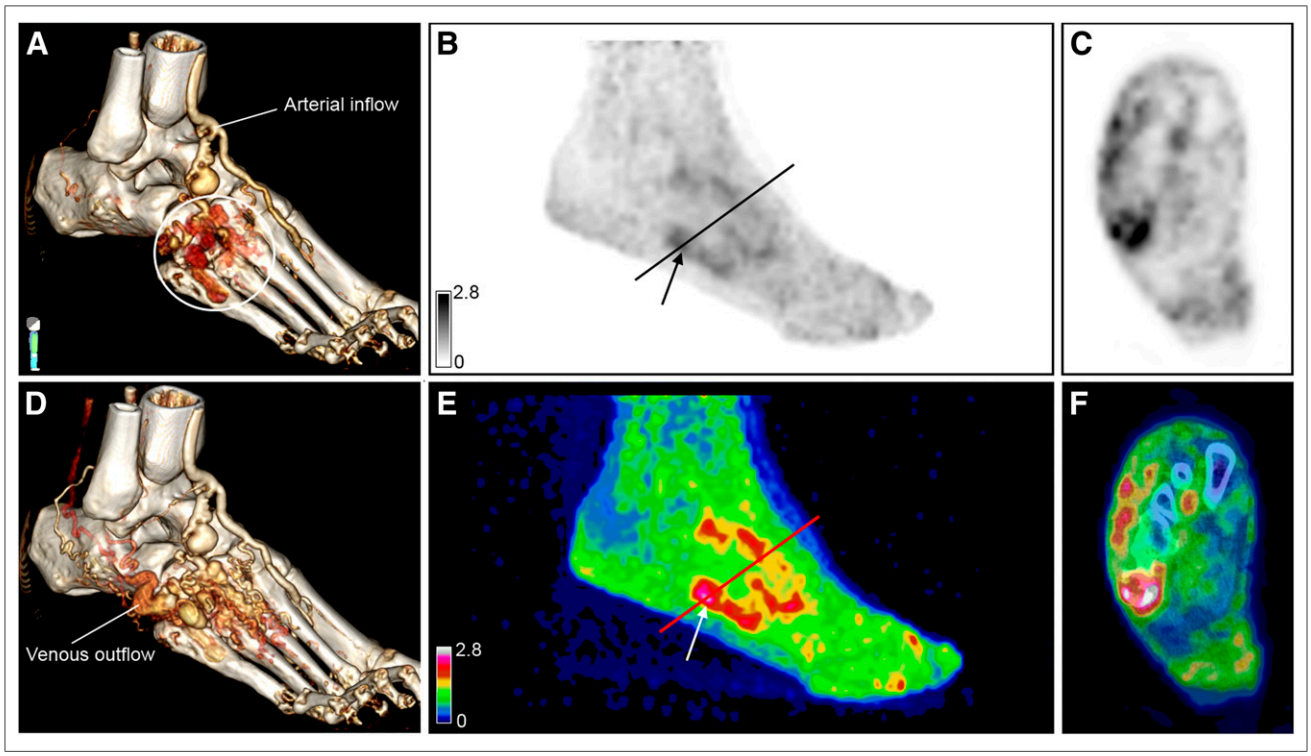

FIGURE 1. A 44-y-old man (patient 3) previously treated with multiple embolizations for symptomatic AVM in distal part of foot. (A and D) Three-dimensional reconstructions of 4D-CTA demonstrate arterial input flow with nidus indicated by white circle (A) and venous outflow (D). (B,C,E,F) Maximum-intensity ^{68}Ga-RGD PET projections at 60 min after injection show uptake (arrows) within lesion (SUV_{max}, 3.0; SUV_{peak}, 2.3). Axial plane in C and F is at location of line in B and E. Lower uptake and a few persistent foci of enhanced activity are seen around toes in E. The arterial and venous flow in this location are not shown in A or D.

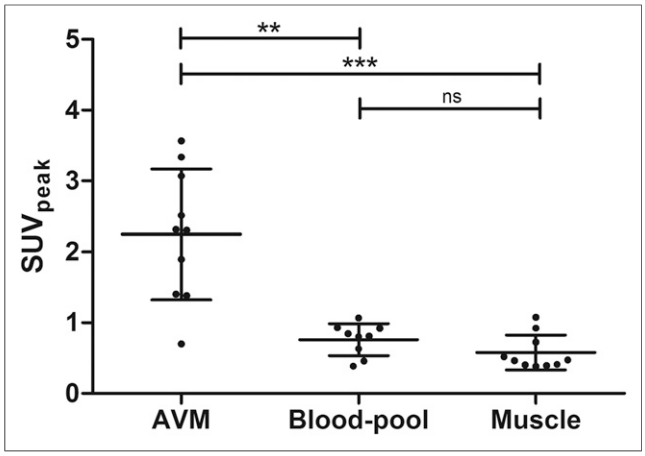

FIGURE 2. Scatterplot of SUV_{peak} of AVM (mean, 2.2 ± 0.9), blood-pool (mean, 0.8 ± 0.2), and muscle activity (mean, 0.6 ± 0.2) for each patient. $^{**}P < 0.005$. $^{***}P < 0.001$. ns = not significant.

In contrast to the low variance in radiotracer uptake in background tissue between patients, a considerable variance in radiotracer uptake was observed within the AVM (Fig. 2). Because all study subjects underwent ^{68}Ga-RGD PET/CT imaging either before the first treatment or between 2 treatments, an exploratory analysis of the correlation between therapy status and ^{68}Ga-RGD uptake was performed (Supplemental Fig. 3).

^{68}Ga-RGD Uptake in Symptomatic and Asymptomatic Lesions

In accord with the presence of pain symptoms near the AVM nidus (symptomatic lesions), ^{68}Ga-RGD PET/CT images revealed enhanced uptake in the tissues adjacent to the nidus in 5 patients (patients 3, 6, 7, 8, and 10), suggesting uptake in asymptomatic lesions as well. In 2 patients (patients 6 and 8), this increased uptake corresponded to an additional nidus also observed on conventional imaging. However, in the other patients, these findings may indicate upregulated integrin $\alpha_v\beta_3$ expression through endothelial cell activation adjacent to the treated nidus, which could not be assessed by conventional imaging (white arrow in Fig. 3A; Supplemental Fig. 4). High uptake was also observed within the intraosseous component of 3 AVMs (patients 3, 7, and 10), as indicated by the yellow arrow in Figure 3B. Patient 3 previously had an extensive symptomatic AVM in the distal part of the foot, which was treated with multiple embolization therapies. The ^{68}Ga-RGD PET/CT images showed significantly lower uptake in the distal part of the foot than in the active nidus in the more proximal part, as well as showing a few persistent foci with enhanced activity around the toes (Fig. 1C), indicating reduced angiogenic activity after treatment.

Immunohistochemical Analysis

Integrin $\alpha_v\beta_3$ expression could be confirmed by immunohistochemical analysis of surgical AVM tissue. Cytoplasmatic and membranous integrin $\alpha_v\beta_3$ expression in endothelial cells of AVMs was observed, showing positive staining both for some arterial endothelial cells (scale, 0–2) and for some venous endothelial cells (scale, 2), as correlated with endothelial cell staining with CD31. In addition, in some tissue samples, expression of integrin $\alpha_v\beta_3$ was observed on erythrocytes (scale, 0–2) and on smooth muscle cells mainly of the vessel walls (scale, 0–1). However, this staining was weak, and background staining could not be excluded. A typical example of the immunostaining is given in Figure 4.

DISCUSSION

This proof-of-concept study showed the feasibility of ^{68}Ga-RGD PET/CT imaging in peripheral AVMs. We demonstrated that ^{68}Ga-RGD uptake is increased in the nidus in patients with AVMs and that this uptake can readily be detected, with good contrast between lesion and background tissue. This good contrast allowed delineation of regions with and without enhanced integrin $\alpha_v\beta_3$ expression within an AVM.

Although the integrin $\alpha_v\beta_3$ expression pattern and its role in tumors, wound healing, and chronic inflammation have already been shown (*16–18*), data on integrin $\alpha_v\beta_3$ expression and its role in AVM have been limited to cerebral vascular malformations (*19*). The angiogenic process in AVM is upregulated by pathologic and physiologic conditions, such as trauma, endothelial shear stress, and immune or inflammatory stimuli (*20,21*). These conditions induce the expression of vascular endothelial growth factors, cytokines (interleukin 6, tumor necrosis factor α), and other endogenous modulators (such as hypoxia-inducible factor 1α), thereby enhancing migration and proliferation of endothelial and smooth-muscle cells, resulting in the formation of new blood vessels (*21*). Immunohistochemical analysis showed endothelial cell expression of $\alpha_v\beta_3$ integrins; however, a more extensive histologic assessment is required to examine potential contributions of extracellular matrix remodeling through activated macrophages, which have been shown to also express $\alpha_v\beta_3$ integrins (*22*). The integrin $\alpha_v\beta_3$ expression pattern on smooth muscle cells and erythrocytes is in line with previous publications (*23*).

In patients with intraosseous involvement, integrin $\alpha_v\beta_3$ was upregulated in those parts of the AVM that showed bone deformation. It is likely that this observed uptake pattern in these patients is due to binding of ^{68}Ga-RGD to integrin $\alpha_v\beta_3$ expressed both on osteoclasts and on endothelial cells, because activated osteoclasts express high

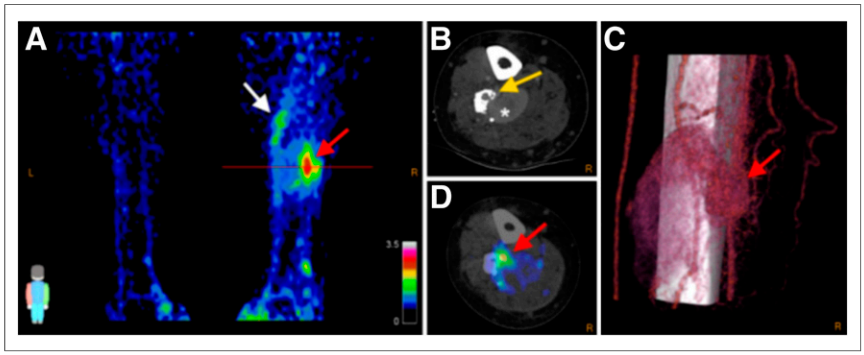

FIGURE 3. A 38-y-old man (patient 7) with right-leg AVM. Maximal-intensity ^{68}Ga-RGD PET projection (A), CTA and ^{68}Ga-RGD PET/CT (B and D), and 3D reconstruction of 4D-CTA (C) show nidus (SUV_{max} 3.2; SUV_{peak} 2.5, red arrows). Axial plane in B and D is at location of line in A. Heterogeneous pattern of enhanced uptake is seen in tissue adjacent to nidus at more proximal part of right leg (white arrow); bone deformation in fibula caused by compression and infiltration of vessels is also seen (yellow arrow), along with large venous aneurysm (asterisk). Arterial flow with nidus and fistula is seen in C, along with upcoming venous flow and the large venous aneurysm.

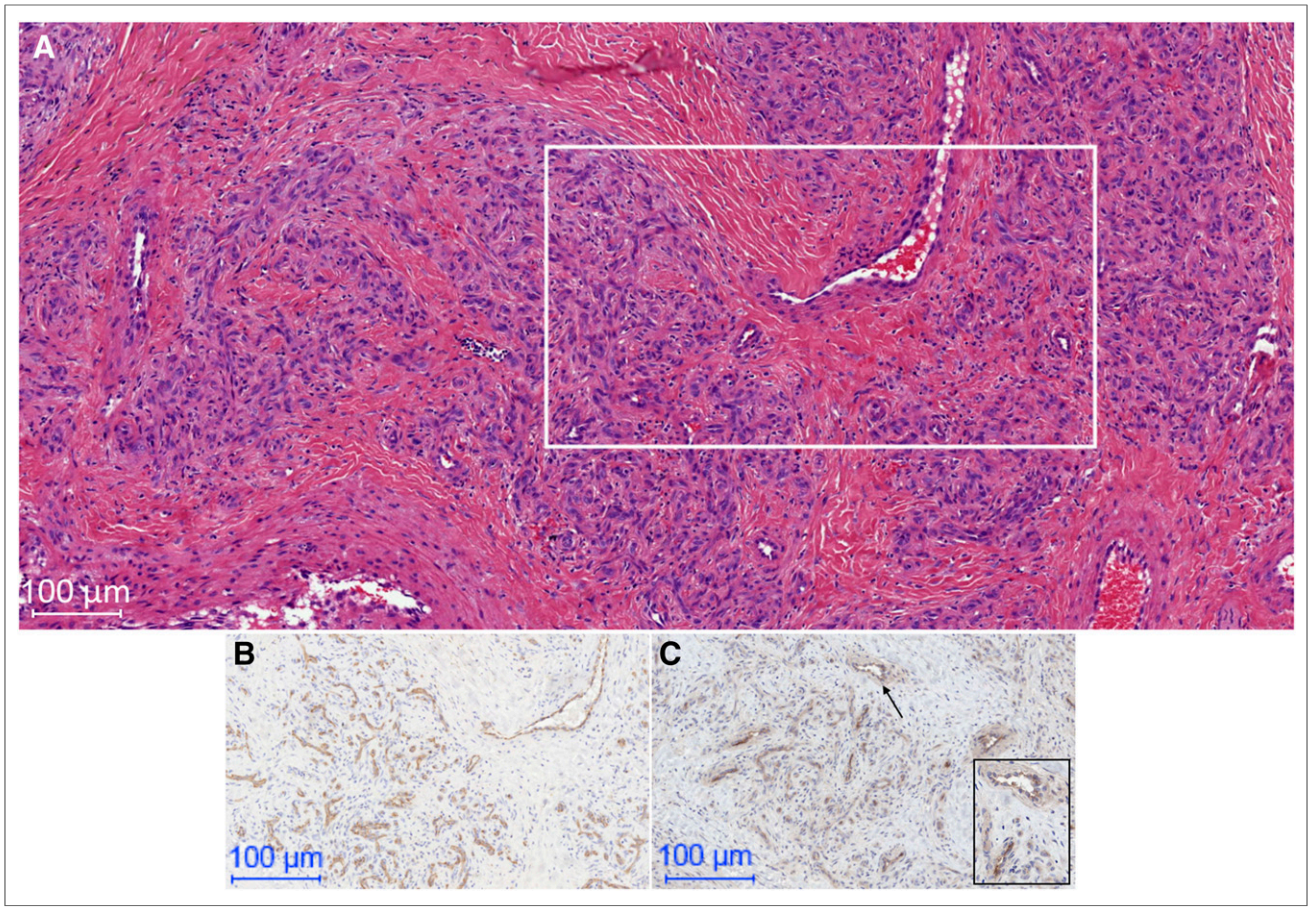

FIGURE 4. An example of immunohistochemical analysis of $\alpha_v\beta_3$ integrin expression for AVM. (A) Hematoxylin- and eosin-stained section, with rectangle indicating region shown in B and C below. (B) Anti-CD31–stained section demonstrating multiple small vessels. (C) Anti-$\alpha_v\beta_3$ integrin–stained section confirming staining of $\alpha_v\beta_3$ integrin of these blood vessels. Rectangle in C is high-power magnification (50 μm) of area indicated by arrow and better shows membranous $\alpha_v\beta_3$ integrin expression in cells of small blood vessels.

amounts of integrin $\alpha_v\beta_3$ to regulate cell–matrix interactions and intracellular signals responsible for bone resorption (*24*). This finding may have consequences for treatment approaches, especially in patients who need clinical follow-up to prevent pathologic fractures.

Although the number of patients included was relatively small, we have made some interesting observations as potential future applications of ^{68}Ga-RGD PET/CT in peripheral AVMs. In 2 patients, ^{68}Ga-RGD PET/CT identified additional foci of integrin $\alpha_v\beta_3$ expression not found on conventional angiographic imaging and, in a complex AVM, ^{68}Ga-RGD PET/CT revealed a clear nidus not seen on conventional imaging. These ^{68}Ga-RGD PET/CT findings may have implications for treatment planning in patients with no clear nidus visible on angiography or patients with a complex or large AVM. Previous studies demonstrated that, for complex AVMs, the lack of standardized and accurate interpretation of images from conventional techniques hampers correct diagnosis and accurate treatment planning (*25*). Furthermore, 4D-CTA and plain angiography provide detailed information on the extent and angioarchitecture of the AVM, but further investigation is needed to evaluate if the angiogenic status of AVM can be used to determine which part of the AVM should be considered as therapeutic target.

There are some limitations of the current feasibility study. Whereas ^{68}Ga-labeled RGD derivatives showed favorable radiochemistry, radiolabeling properties, and tumor–to–normal-tissue ratios (*12*), the image resolution of ^{68}Ga-labeled radiotracers is generally inferior to that of ^{18}F-labeled radiotracers (*26*). Furthermore, a contribution from nonspecific uptake to ^{68}Ga-RGD accumulation cannot be excluded, but because RGD radiotracers have shown rapid clearance from the circulation, the enhanced permeability and retention effect is unlikely to play a major role in these lesions. Another limitation is that only 1 time point per patient was acquired. Therefore, an appropriate statistical analysis of the changes in angiogenesis before and after embolization was not feasible. Longitudinal ^{68}Ga-RGD PET/CT scans within the same patient—acquired in combination with conventional imaging, at baseline and during the course of embolization treatment—would be needed to investigate whether ^{68}Ga-RGD PET/CT can predict the response to therapy.

A few case reports have reported a role for novel antiangiogenic therapeutics in peripheral AVMs (*27–29*). The expression of integrin $\alpha_v\beta_3$ in peripheral AVMs paves the way to further evaluation of antiangiogenic treatments for AVMs and the role of ^{68}Ga-RGD PET/CT in the development of these therapies. Besides, ^{68}Ga-RGD PET/CT imaging may have the potential to provide quantitative information on the underlying pathogenesis of AVMs. New prospective clinical trials are warranted to determine how this novel imaging technique can improve our understanding of angiogenesis in AVMs and, furthermore, how ^{68}Ga-RGD PET/CT can be used to investigate its potential to personalize treatment of AVM patients.

CONCLUSION

In this study, we demonstrated the feasibility of using ^{68}Ga-RGD PET/CT imaging to visualize integrin $\alpha_v\beta_3$ expression in peripheral AVMs. ^{68}Ga-RGD PET/CT may provide important information complementary to that from conventional angiography and potentially be a valuable tool for the assessment of angiogenesis. These findings will stimulate further studies on the exact role of angiogenesis in AVMs. Such studies are needed to investigate the potential role of ^{68}Ga-RGD PET/CT in managing AVMs or in guiding treatments with novel drugs targeting angiogenesis.

DISCLOSURE

Daphne Lobeek is supported by grant 95104005 from The Netherlands Organisation for Health Research and Development (ZonMW). Ha-Long Nguyen received a Pierre M. fellowship. Samantha Terry is supported by the Wellcome/EPSRC Centre for Medical Engineering [WT 203148/Z/16/Z], King's College London, the UCL Comprehensive Cancer Imaging Centre, and the CRUK and EPSRC in association with the MRC and DoH (England). Laurence Boon is in part supported by FNRS grant T.0146.16 from the Fonds de la Recherche Scientifique. Miikka Vikkula, Laurence Boon, Willemijn Klein, and Leo Schultze Kool are members of the Vascular Anomalies Working Group of the European Reference Network (VASCERN, project 769036). No other potential conflict of interest relevant to this article was reported.

ACKNOWLEDGMENTS

We thank the colleagues of the Radiopharmacy of the Department of Radiology and Nuclear Medicine and the Department of Pharmacy for helping to prepare the radiopharmaceuticals. We also thank Willem-Jan van der Woude, Peter J.M. Kok, Michel de Groot, Judith J.F. Thijssen, Marti Boss, and Viviane C.J. van de Crommert for helping to screen the patients or work up the ^{68}Ga-RGD PET/CT scans, and we thank Roel W. Ten Broek and Louis Libbrecht for helping with immunohistology.

KEY POINTS

QUESTION: Can ^{68}Ga-RGD PET/CT imaging be used to visualize angiogenesis in peripheral AVMs?

PERTINENT FINDINGS: This proof-of-concept study showed that ^{68}Ga-RGD PET/CT enables visualization of $\alpha_v\beta_3$ integrins in peripheral AVMs. Tracer uptake was significantly higher in AVMs than in background tissue, with lesion-to-blood and lesion-to-muscle ratios of 3.5 ± 2.2 and 4.6 ± 2.8, respectively.

IMPLICATIONS FOR PATIENT CARE: Future studies may reveal whether ^{68}Ga-RGD PET/CT may act as a molecular imaging technique complementary to the existing imaging modalities and guide the application of novel antiangiogenic drugs in peripheral AVMs.

REFERENCES

1. Cordisco MR. Part IIID: arteriovenous malformations. In: Cordisco MR, ed. *Vascular Anomalies in Childhood.* Buenos Aires, Argentina: Pierre Fabre Dermatologie; 2016:244–356.
2. Lu L, Bischoff J, Mulliken JB, Bielenberg DR, Fishman SJ, Greene AK. Increased endothelial progenitor cells and vasculogenic factors in higher-staged arteriovenous malformations. *Plast Reconstr Surg.* 2011;128:260e–269e.
3. Rangel-Castilla L, Russin JJ, Martinez-Del-Campo E, Soriano-Baron H, Spetzler RF, Nakaji P. Molecular and cellular biology of cerebral arteriovenous malformations: a review of current concepts and future trends in treatment. *Neurosurg Focus.* 2014;37:E1.
4. Ogilvy CS, Stieg PE, Awad I, et al. Recommendations for the management of intracranial arteriovenous malformations: a statement for healthcare professionals from a special writing group of the Stroke Council, American Stroke Association. *Circulation.* 2001;103:2644–2657.
5. Lee BB, Baumgartner I, Berlien HP, et al. Consensus document of the International Union of Angiology (IUA)-2013: current concept on the management of arterio-venous management. *Int Angiol.* 2013;32:9–36.
6. Do YS, Yakes WF, Shin SW, et al. Ethanol embolization of arteriovenous malformations: interim results. *Radiology.* 2005;235:674–682.
7. Walker EJ, Su H, Shen F, et al. Bevacizumab attenuates VEGF-induced angiogenesis and vascular malformations in the adult mouse brain. *Stroke.* 2012;43:1925–1930.
8. Colletti G, Dalmonte P, Moneghini L, Ferrari D, Allevi F. Adjuvant role of antiangiogenic drugs in the management of head and neck arteriovenous malformations. *Med Hypotheses.* 2015;85:298–302.
9. Haubner R, Maschauer S, Prante O. PET radiopharmaceuticals for imaging integrin expression: tracers in clinical studies and recent developments. *BioMed Res Int.* 2014;2014:871609.
10. Hong H, Chen F, Zhang Y, Cai W. New radiotracers for imaging of vascular targets in angiogenesis-related diseases. *Adv Drug Deliv Rev.* 2014;76:2–20.
11. Lobeek D, Franssen GM, Ma MT, et al. In vivo characterization of 4 ^{68}Ga-labeled multimeric RGD peptides to image $\alpha_v\beta_3$ integrin expression in 2 human tumor xenograft mouse models. *J Nucl Med.* 2018;59:1296–1301.
12. Dijkgraaf I, Yim CB, Franssen GM, et al. PET imaging of $\alpha_v\beta_3$ integrin expression in tumours with ^{68}Ga-labelled mono-, di- and tetrameric RGD peptides. *Eur J Nucl Med Mol Imaging.* 2011;38:128–137.
13. Arrieta O, Garcia-Perez FO, Michel-Tello D, et al. Response assessment of ^{68}Ga-DOTA-E-[c(RGDfK)]^2 PET/CT in lung adenocarcinoma patients treated with nintedanib plus docetaxel. *J Nucl Med.* 2018;59:403–409.
14. Terry SY, Abiraj K, Frielink C, et al. Imaging integrin $\alpha_v\beta_3$ on blood vessels with ^{111}In-RGD$_2$ in head and neck tumor xenografts. *J Nucl Med.* 2014;55:281–286.
15. Yakes WF, Vogelzang RL, Ivancev K, Yakes AM. New arteriographic classification of AVM based on the Yakes classification system. In: Kim YW, Lee BB, Yakes WF, YS, eds. *Congenital Vascular Malformations.* New York, NY: Springer; 2017.
16. Desgrosellier JS, Cheresh DA. Integrins in cancer: biological implications and therapeutic opportunities. *Nat Rev Cancer.* 2010;10:9–22.
17. Schnittert J, Bansal R, Storm G, Prakash J. Integrins in wound healing, fibrosis and tumor stroma: high potential targets for therapeutics and drug delivery. *Adv Drug Deliv Rev.* 2018;129:37–53.
18. Avraamides CJ, Garmy-Susini B, Varner JA. Integrins in angiogenesis and lymphangiogenesis. *Nat Rev Cancer.* 2008;8:604–617.
19. Lim M, Haddix T, Harsh GR, Vogel H, Steinberg GK, Guccione S. Characterization of the integrin αvβ3 in arteriovenous malformations and cavernous malformations. *Cerebrovasc Dis.* 2005;20:23–27.
20. Buell TJ, Ding D, Starke RM, Webster Crowley R, Liu KC. Embolization-induced angiogenesis in cerebral arteriovenous malformations. *J Clin Neurosci.* 2014;21:1866–1871.
21. Mouchtouris N, Jabbour PM, Starke RM, et al. Biology of cerebral arteriovenous malformations with a focus on inflammation. *J Cereb Blood Flow Metab.* 2015;35:167–175.
22. Antonov AS, Antonova GN, Munn DH, et al. αVβ3 integrin regulates macrophage inflammatory responses via PI3 kinase/Akt-dependent NF-κB activation. *J Cell Physiol.* 2011;226:469–476.
23. Max R, Gerritsen RR, Nooijen PT, et al. Immunohistochemical analysis of integrin αvβ3 expression on tumor-associated vessels of human carcinomas. *Int J Cancer.* 1997;71:320–324.
24. Nakamura I, Duong LT, Rodan SB, Rodan GA. Involvement of $\alpha_v\beta_3$ integrins in osteoclast function. *J Bone Miner Metab.* 2007;25:337–344.
25. Madani H, Farrant J, Chhaya N, et al. Peripheral limb vascular malformations: an update of appropriate imaging and treatment options of a challenging condition. *Br J Radiol.* 2015;88:20140406.
26. Sanchez-Crespo A. Comparison of gallium-68 and fluorine-18 imaging characteristics in positron emission tomography. *Appl Radiat Isot.* 2013;76:55–62.
27. Bauditz J, Lochs H. Angiogenesis and vascular malformations: antiangiogenic drugs for treatment of gastrointestinal bleeding. *World J Gastroenterol.* 2007;13:5979–5984.
28. Pföhler C, Janssen E, Buecker A, Vogt T, Muller CS. Successful treatment of a congenital extra-truncal vascular malformation by orally administered propranolol. *J Dermatolog Treat.* 2015;26:59–62.
29. Burrows PE, Mulliken JB, Fishman SJ, Klement GL, Folkman J. Pharmacological treatment of a diffuse arteriovenous malformation of the upper extremity in a child. *J Craniofac Surg.* 2009;20(suppl 1):597–602.